Int. J. Heat Mass Transfer. Vol. 12, pp. 1267–1279. Pergamon Press 1969. Printed in Great Britain

FLOW DEVELOPMENT IN A TUBE WITH INJECTION OF A LIGHT OR HEAVY GAS†

P. A. LIBBY, T. M. LIU and F. A. WILLIAMS

Department of the Aerospace and Mechanical Engineering Sciences, University of California, San Diego, La Jolla, California

(*Received* 1 *November* 1968 *and in revised form* 3 *March* 1969)

Abstract—Laminar isothermal entrance flows in ducts of circular cross section with uniform rate of mass injection at the wall are calculated from the boundary-layer equations by an implicit finite-difference technique. Results are reported for systems with constant molecular weight, for injection of a light gas into a heavy gas, and for injection of a heavy gas into a light gas, with special emphasis on helium–nitrogen mixtures. Dependence of density and viscosity on composition is properly taken into account. The effect of molecular weight on flow development and mixing is discussed.

NOMENCLATURE

a, radius of the tube;
$\mathscr{M}$, $\rho\mathscr{D}_{12}/\mu_0$, cf. equation (7);
$\bar{r}$, r/a, normalized radial coordinate;
R, Reynolds number based on entrance properties, $\rho_0 u_0 a/\mu_0 = \rho_1 u_0 a/u_1$;
$\bar{u}, \bar{v}$, velocity components in x, r directions normalized by uniform entrance velocity, respectively;
V, $\bar{\rho}\bar{v}\bar{r}$;
w_1, $(W_1/W_2) - 1$;
W_1, molecular weight of species 1;
W_2, molecular weight of species 2;
$\bar{x}$, x/a, normalized axial coordinate;
$\tilde{x}$, $\bar{x}/R$, scaled axial coordinate.

Greek symbols

κ, mass fraction of injected species;
$\bar{\mu}$, viscosity normalized by entrance viscosity, cf. equation (7);
$\bar{\rho}$, mass density normalized by entrance mass density;
σ_1, molecular diameters of species 1;
σ_2, molecular diameters of species 2;
σ_{12}, average molecular diameters, cf. equation (7).

Subscripts

c, conditions in the coolant chamber;
e, conditions in the external flow;
w, conditions at the wall, $\bar{r} = 1$.

1. INTRODUCTION

FLOW development in ducts has been the subject of extensive theoretical and experimental study. Motivation for such work stems from numerous design problems that arise in chemical engineering, in mechanical engineering, and more recently in aerospace applications such as engine inlet flow, flow in combustion chambers, transpiration cooling of internal flows, etc. The majority of the applications involve turbulent flow, but many instances arise (e.g., in flight at high altitudes) wherein the Reynolds number is low enough for laminar conditions to prevail. The present investigation concerns a particular class of internal laminar flows.

Theoretical analyses of developing flows in ducts are relatively difficult to perform. Unlike Poiseuille flow, boundary layers, lubrication flows, etc., developing duct flows present both non-linearities (due to the presence of inertial as

† This research was sponsored by the Air Force Office of Scientific Research, Office of Aerospace Research, United States Air Force, under Grant No. AF-AFOSR-927A-67.

well as viscous and pressure forces) and streamwise-dependent effects (e.g., an axial pressure gradient which is not known in advance) that because of the specified geometry cannot be simplified or removed by the usual transformations of variables (e.g., the Levy–Lees transformation). Thus, two types of approaches are available for analyzing developing internal flows theoretically: one is to employ approximate techniques based on series expansions about known upstream and/or downstream conditions, based on Karman–Pohlhausen integral-type methods, or based on various approximate linearizations of the conservation equations. The other is to employ electronic computers for solving finite-difference forms of the conservation equations. The accuracy of results obtained from the first type of approach can properly be judged only by comparison either with results of the second approach or with experiment, since numerical techniques are generally conceded to be the more accurate (and also more laborious) of the two types of theoretical methods. The present theoretical analysis employs the more accurate, finite-difference approach. A series expansion about upstream conditions is also developed, for the purpose of starting the finite-difference calculation.

With few exceptions, finite-difference calculations of duct flows have been based on the boundary-layer approximation. Under most conditions the boundary-layer approximation is known to be imprecise in certain regions of the flow; for example, when the entrance velocity profile is taken to be uniform, boundary-layer theory yields the unacceptable result that the pressure gradient is infinite at the entrance plane of a duct. Nevertheless, heuristic justifications exist for using boundary-layer theory in the down stream portion of a slender duct for both high and moderate Reynolds numbers, and it is commonly accepted that the boundary-layer equations describe the flow field correctly everywhere except in specific regions, such as the upstream potential core, which can be identified with reasonable confidence. Furthermore, in converting the mathematical problem from an elliptic one to a parabolic one, the boundary-layer approximation introduces appreciable simplification into a finite-difference calculation by making it possible to begin at the entrance to the duct and to calculate the solution by marching downstream. The boundary-layer equations are employed in the present theory.

Hornbeck [1] calculated the imcompressible flow field in a pipe of circular cross section, with constant density and viscosity, for the case in which the inlet velocity profile was uniform. He employed a backward difference scheme that involved solving a set of linear algebraic equations at each axial step in the mesh. Later, Hornbeck, Rouleau and Osterle [2] extended this method by calculating some flows with uniform and nonuniform rates of injection and suction at the wall, for cases with both parabolic and uniform initial velocity profiles. In the present study, the species conservation equation is appended to the set of conservation equations used in [1, 2], variations of density and viscosity due to concentration variations in isothermal, incompressible flows are properly taken into account, and an implicit iterative scheme for solving the finite-difference equations at each axial step is used for calculating entrance flows in circular ducts with uniform rates of mass injection of a foreign gas at the wall, for the case in which the inlet velocity profile is uniform.

The interest in wall injection of foreign gases stems from their effects on mass and momentum transport processes which in turn may affect the characteristics and the length of the flow development zone. For example, injection of a light gas into a flat-plate boundary layer is known to modify the wall shear and mass transfer coefficient appreciably; boundary-layer profiles with inflection points can develop for injection on a flat plate; it is of interest to investigate whether a similar phenomenon can occur in ducts. Extensions of the present calculations to nonisothermal systems can reveal the effect of the molecular weight of the injected

species on the heat protection afforded the wall by injection.

2. ANALYSIS

The flow under consideration is shown schematically in Fig. 1. A porous cylindrical

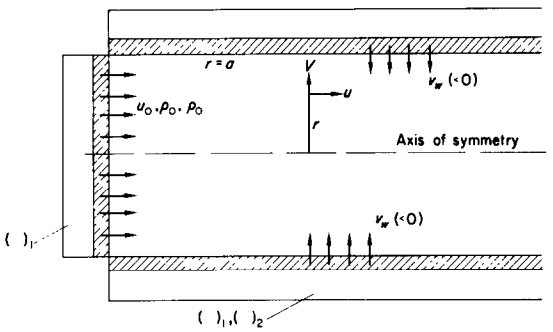

FIG. 1. Schematic representation of the flow.

tube is closed at one end by a porous disc. Each porous surface is jacketed so as to permit the injection of gases and gas mixtures through them. We consider the case wherein a pure gas denoted by a subscript 1 is injected through the porous disc and wherein a second gas denoted with a subscript 2, perhaps in a mixture of gas 1, is injected through the cylindrical surface. Although our numerical work will assume uniform mass transfer through both surfaces, the analysis and numerical techniques are sufficiently general so that arbitrarily distributed mass transfer through the cylindrical surface may be treated. Of course in this case the porosity of the cylinder must be assumed variable in the streamwise direction. We shall assume that the entire system is isothermal and low speed; thus the gas density will depend only on composition.

2.1 *Describing equations*

The describing equations in nondimensional form are

$$\bar{\rho}\bar{u}\frac{\partial \bar{u}}{\partial \bar{x}} + \bar{\rho}\bar{v}\frac{\partial \bar{u}}{\partial \bar{r}} = -\frac{\partial \bar{p}}{\partial \bar{x}} + \frac{1}{R\bar{r}}\frac{\partial}{\partial \bar{r}}\left(\bar{\mu}\bar{r}\frac{\partial \bar{u}}{\partial \bar{r}}\right), \tag{1}$$

$$\frac{\partial \bar{p}}{\partial \bar{r}} = 0, \tag{2}$$

$$\bar{\rho}\frac{\partial \bar{u}}{\partial \bar{x}} + \bar{u}\frac{\partial \bar{\rho}}{\partial \bar{x}} + \frac{1}{\bar{r}}\frac{\partial}{\partial \bar{r}}(\bar{\rho}\bar{v}\bar{r}) = 0, \tag{3}$$

$$\bar{\rho}\bar{u}\frac{\partial \kappa}{\partial \bar{x}} + \bar{\rho}\bar{v}\frac{\partial \kappa}{\partial \bar{r}} = \frac{1}{R\bar{r}}\frac{\partial}{\partial \bar{r}}\left(\mathscr{M}\bar{r}\frac{\partial \kappa}{\partial \bar{r}}\right), \tag{4}$$

where the symbols are defined in the Nomenclature; for clarity we repeat here that $R \equiv \rho_0 u_0 a/\mu_0$, a Reynolds number defined in terms of the flow at the plane $x \sim \bar{x} = 0$; that $\mathscr{M} \equiv \rho\mathscr{D}_{12}/\mu_0$, a diffusion parameter; and that κ is the mass fraction of gas 2 injected through the cylindrical surface. We note that the assumptions of only gas 1 being injected through the disc and of isothermal conditions imply that the reference quantities ρ_0, μ_0 may be replaced by ρ_1, μ_1, respectively. However, to provide for more general cases we retain the more general reference quantities.

The boundary and initial conditions to be imposed on equations (1)–(4) are

$$\begin{aligned} &\bar{u}(0,\bar{r}) = 1, \quad \bar{r} < 1; \quad \bar{p}(0) = 1 \\ &\bar{u}(\bar{x},1) = 0; \quad (\bar{\rho}\bar{v})(\bar{x},1) = (\rho v)_w, \quad \text{given}; \\ &\partial\kappa/\partial\bar{r}\,(\bar{x},0) = (R/\mathscr{M})(\bar{\rho}\bar{v})_w(\kappa_c - \kappa_w). \end{aligned} \tag{5}$$

In addition certain regularity conditions at $\bar{r} = 0$, i.e., at the axis of symmetry must be imposed, leading to

$$\left.\begin{aligned} &\lim_{\bar{r}\to 0}(1/\bar{r})(\partial/\partial\bar{r})\left[\bar{\mu}\bar{r}(\partial\bar{u}/\partial\bar{r})\right] = 2\bar{\mu}(\partial^2\bar{u}/\partial\bar{r}^2)\big|_{\bar{r}=0} \\ &\lim_{\bar{r}\to 0}(1/\bar{r})(\partial/\partial\bar{r})\left[\mathscr{M}\bar{r}(\partial\kappa/\partial\bar{r})\right] \\ &\qquad = 2\mathscr{M}(\partial^2\kappa/\partial\bar{r}^2)\big|_{\bar{r}=0} \\ &\lim_{\bar{r}=0}(1/\bar{r})(\partial\kappa/\partial\bar{r}) = (\partial^2\kappa/\partial\bar{r}^2)\big|_{\bar{r}=0} \end{aligned}\right\} \tag{6}$$

Although the initial conditions stated above are sufficient in principle, the imposition of the step condition on $\bar{u}$ at $\bar{x} = 0$ as $\bar{r} \to 1$ suggests that a special analytic treatment of the initial data is required. Accordingly, in the Appendix

we present an analysis which provides initial data at a finite, small value of $\bar{x}$ and which should be considered an extension to injection, either homogeneous or heterogeneous, of the analysis of Atkinson and Goldstein [5]. This, in fact, has been used in the numerical work below.

The last of equations (5) derives from conservation of gas 2 between the exposed surface $\bar{r} = 1$ and a surface within the jacket surrounding the cylinder; note in this equation that κ_c is the mass fraction of species 2 in this jacket. If $\kappa_c = 0$, then we are treating a homogeneous case, only gas 1 being injected through the disc and cylinder.

2.2 *The transport properties*

We use for the description of the transport properties the following semi-empirical equations [3] which prevail for our isothermal flow:

$$\left.\begin{aligned}
&\bar{u} \equiv \mu/\mu_0 = \{1 + 1{\cdot}385\,(w_1 + 1)\,[\kappa/(1-\kappa)] \\
&\times (1 + \kappa w_1)]\,(1/\mathscr{M})\}^{-1} + (\mu_2/\mu_0) \\
&\times \{1 + 1{\cdot}385\,(\mu_2/\mu_0)\,[(1-\kappa)/\kappa(1+\kappa w_1)] \\
&\times (1/\mathscr{M})\}^{-1} \\
&\mathscr{M} = \rho\mathscr{D}_{12}/\mu_0 = 6/5(\sigma_1/\sigma_{12})^2(W/W_1) \\
&\times [(W_1 + W_2)/2W_2]^{\frac{1}{2}} \\
&\mu_2/\mu_0 = \sigma_1^2/\sigma_2^2(W_2/W_1)^{\frac{1}{2}} \\
&W/W_1 = (\kappa w_1 + 1)^{-1} \\
&\sigma_{12} = (\sigma_1 + \sigma_2)/2.
\end{aligned}\right\} \quad (7)$$

Thus we see that the transport properties are determined to the approximations employed here by the molecular diameters and molecular weights σ_i, W_i, respectively. For the calculations presented below the binary system of nitrogen and helium is considered; we have used the molecular and transport data given in Table 1.

Table 1

	He	N_2
W(g/mole)	4	28
μ(g/cm s)	1981	1786
σ(Å)	1·90	3·36

2.3 *The equation of state*

Consistent with the assumptions of isothermal and low-speed flow, the equations of state yield

$$\bar{\rho} \equiv \rho/\rho_0 = (\kappa w_1 + 1)^{-1}. \quad (8)$$

In the course of the development below we shall need

$$\partial\bar{\rho}/\partial\bar{x} = -\bar{\rho}^2 w_1(\partial\kappa/\partial\bar{x}). \quad (9)$$

2.4 *Rearrangement of equations*

We next rearrange equations (1)–(4) so as to put them in a form suitable for numerical treatment: our basic approach is to determine $(\partial\bar{u}/\partial\bar{x})$ and $(\partial\kappa/\partial\bar{x})$ in terms of the dynamic and state variables at a given station, and to use them to make estimates of $\bar{u}$ and κ at an advanced station. From these the $\bar{v}$-velocity is estimated at the advanced station and we are in position to refine our calculations by iteration, i.e., to calculate more accurately $\bar{u}$, κ and $\bar{v}$ at the advanced station.

From equations (3), (4) and (9) it is easy to show that

$$\frac{\partial\bar{u}}{\partial\bar{x}} = -\frac{1}{\bar{\rho}\bar{r}}\frac{\partial V}{\partial\bar{r}} + \left(\frac{w_1}{\bar{\rho}^2}\right)\left[\frac{V}{\bar{r}}\frac{\partial\kappa}{\partial\bar{r}} - \frac{1}{R\bar{r}}\frac{\partial}{\partial\bar{r}}\left(\mathscr{M}\bar{r}\frac{\partial\kappa}{\partial\bar{r}}\right)\right], \quad (10)$$

$$\frac{\partial\kappa}{\partial\bar{x}} = -\left[V\left(\frac{\partial\kappa}{\partial\bar{r}}\right) - \frac{1}{R}\frac{\partial}{\partial\bar{r}}\left(\mathscr{M}\bar{r}\frac{\partial\kappa}{\partial\bar{r}}\right)\right](\bar{\rho}\bar{u}\bar{r})^{-1}. \quad (11)$$

Now if equation (1) is differentiated with respect to $\bar{r}$ so as to eliminate $\bar{p}$, if equation (10) is also differentiated with respect to $\bar{r}$, and if $(\partial^2\bar{u}/\partial\bar{x}\partial\bar{r})$ is eliminated between the two resulting equations, there is obtained

$$\begin{aligned}
&\partial^2 V/\partial\bar{r}^2 + [w_1\bar{\rho}(\partial\kappa/\partial\bar{r}) - 1/\bar{r}]\partial V/\partial\bar{r} \\
&+ [w_1\bar{\rho}/\bar{u}(\partial\bar{u}/\partial\bar{r})\,(\partial\kappa/\partial\bar{r}) - w_1\bar{\rho}/\bar{r}(\partial\kappa/\partial\bar{r}) \\
&- w_1^2\bar{\rho}^2(\partial\kappa/\partial\bar{r})^2 + w_1\bar{\rho}(\partial^2\kappa/\partial\bar{r}^2) \\
&+ 1/\bar{u}\bar{r}(\partial\bar{u}/\partial\bar{r}) - 1/\bar{u}(\partial^2\bar{u}/\partial\bar{r}^2)]V \\
&= \{w_1\bar{\rho}[1/\bar{u}(\partial\bar{u}/\partial\bar{r}) - w_1\bar{\rho}(\partial\kappa/\partial\bar{r}) - 1/\bar{r}].
\end{aligned}$$

$$- \partial/\partial\bar{r}[\mathscr{M}\bar{r}(\partial\kappa/\partial\bar{r})] + w_1\bar{\rho}(\partial^2/\partial\bar{r}^2)[\mathscr{M}\bar{r}(\partial\kappa/\partial\bar{r})] + 1/\bar{u}\bar{r}(\partial/\partial\bar{r})[\bar{\mu}\bar{r}(\partial\bar{u}/\partial\bar{r}) - 1/\bar{u}(\partial^2/\partial\bar{r}^2)[\bar{\mu}\bar{r}(\partial\bar{u}/\partial\bar{r})]\}R^{-1}. \quad (12)$$

We consider equations (10)–(12) to provide the basis for numerical analysis; symbolically we have

$$\partial\bar{u}/\partial\bar{x} = G(\kappa, V) \quad (10a)$$

$$\partial\kappa/\partial\bar{x} = H(\bar{u}, \kappa, V) \quad (11a)$$

$$\partial^2 V/\partial\bar{r}^2 + L(\bar{u}, \kappa)\partial V/\partial\bar{r} + M(\bar{u}, \kappa)V = N(\bar{u}, \kappa). \quad (12a)$$

There are several ways in which this set of equations can be handled numerically; we have used a higher order implicit scheme based on iteration. The k-th iterate for $\bar{u}$, and κ at a value of $\bar{x}$ and $\bar{r}$ identified by the indices n, m are given by

$$^{(k)}\bar{u}^{n,m} = \bar{u}^{n-1,m} + (G^{n-1,m} + {}^{(k-1)}G^{n,m})(1/2)(\bar{x}^n - \bar{x}^{n-1})$$

$$^{(k)}\kappa^{n,m} = \kappa^{n-1,m} + (H^{n-1,m} + {}^{(k-1)}H^{n,m})(1/2)(\bar{x}^n - \bar{x}^{n-1}).$$

The $\bar{r}$-derivatives appearing in G and H are approximated by finite differences with a uniform grid of spacing $\delta_{\bar{r}}$; the first approximations to $G^{n,m}$, $H^{n,m}$, i.e., the approximations used for $k = 1$, are the values at the previous station; more precisely, we take $^{(0)}G^{n,m} = G^{n-1,m}$, $^{(0)}H^{n,m} = H^{n-1,m}$. Equation (12a), put in finite difference form, results in a tridiagonal matrix whose solution by a standard algorithm yields the k-th iterate for the V's at the station identified by the index n. Again the $\bar{r}$-derivatives appearing in L, M, N are approximated by finite differences.

To give some indication of the difference representations used we write two typical cases below:

$$\left[\frac{\partial}{\partial\bar{r}}\left(\mathscr{M}\bar{r}\frac{\partial\kappa}{\partial\bar{r}}\right)\right]^{n,m} = \left(\frac{1}{\delta_{\bar{r}}^2}\right)\left[\left(\mathscr{M}\bar{r}\frac{\partial\kappa}{\partial\bar{r}}\right)^{n,m+1/2} - \left(\mathscr{M}\bar{r}\frac{\partial\kappa}{\partial\bar{r}}\right)^{n,m-1/2}\right]$$

$$= \left(\frac{1}{\delta_{\bar{r}}^2}\right)\left[(\mathscr{M}\bar{r})^{n,m+1/2}(\kappa^{n,m+1} - \kappa^{n,m}) - (\mathscr{M}\bar{r})^{n,m-1/2}(\kappa^{n,m} - \kappa^{n-1})\right],$$

$$\left[\frac{\partial^2}{\partial\bar{r}^2}\left(\bar{\mu}\bar{r}\frac{\partial\bar{u}}{\partial\bar{r}}\right)\right]^{n,m} = \left(\frac{1}{\delta_{\bar{r}}^2}\right)\left[\bar{\mu}\bar{r}\frac{\partial\bar{u}}{\partial\bar{r}}^{n,m+1} - 2\left(\bar{\mu}\bar{r}\frac{\partial\bar{u}}{\partial\bar{r}}\right)^{n,m} + \left(\bar{\mu}\bar{r}\frac{\partial\bar{u}}{\partial r}\right)^{n,m-1}\right]$$

$$= \frac{1}{2\delta_{\bar{r}}^3}[(\bar{\mu}\bar{r})^{n,m+1}(\bar{u}^{n,m+2} - \bar{u}^{n,m}) - 2(\bar{\mu}\bar{r})^{n,m}(\bar{u}^{n,m+1} - \bar{u}^{n,m-1}) + (\bar{\mu}\bar{r})^{n,m-1}(\bar{u}^{n,m} - \bar{u}^{n,m-2})]$$

where $(\ )^{n,m+1/2} = (1/2)[(\ )^{n,m+1} + (\ )^{n,m}]$.

To implement this computing scheme there must be solved the usual problems of special finite difference forms for the grid points near the boundaries; of the determination of the $\bar{x}$-wise step size; and of the number of iterations to be undertaken. The first mentioned problem is straightforward; the latter two are discussed below.

2.5 *Determination of the pressure*

Once the velocity and composition fields are determined the pressure distribution $\bar{p} = \bar{p}(\bar{x})$ may be computed in several ways; we have used equation (1) evaluated at the wall of the tube. In nondimensional form this leads to

$$-\frac{\partial\bar{p}}{\partial\bar{x}} = V_w\left(\frac{\partial\bar{u}}{\partial\bar{r}}\right)_{\bar{r}=1} - \frac{1}{R}\left[\frac{\partial}{\partial\bar{r}}\bar{\mu}\bar{r}\left(\frac{\partial\bar{u}}{\partial\bar{r}}\right)\right]_{r=1} \quad (13)$$

If $\bar{p} = \bar{p}(\bar{x})$ is desired, equation (13) may be integrated with the initial condition $\bar{p}(0) = 1$.

2.6 *The asymptotic behaviour for the homogeneous case*

In making comparison of our calculations with

previous results for the homogeneous case it will be convenient to consider the far-downstream behaviour. Yuan [4] has shown that the velocity profile in the region remote from the entrance is given by

$$\bar{u}/\bar{u}_e = \cos(\pi\bar{r}^2/2) \tag{14}$$

where $\bar{u}_e = \bar{u}(\bar{x}, 0)$, the normalized centerline velocity. Equation (14) will also apply for the nonhomogeneous case when the distance downstream is sufficiently large for the concentration of species 1 to be negligibly small.

2.7 *Remarks on the numerical techniques*

Except for the region close to the origin $\bar{x} = 0$ where a fine mesh was required as described in the Appendix, all the results presented below, were obtained with a uniform mesh size in the $\bar{r}$ direction such that $\delta_{\bar{r}} = 1/80$ and $1/20$; the $(1/40)$ value was found to provide accurate results without excessive computing time. We note that $\delta_{\bar{r}} = 1/40$ is approximately equal to the smallest mesh size that was found to be needed in [1] and [2] for assuring accuracy near the inlet and near the wall. The step size in the $\bar{x}$-direction was variable in our program and self-determined as an integral part of the iteration scheme. Assume that a satisfactory $\Delta_{\bar{x}}$ has been found and the solution determined at a certain station $\bar{x} = \bar{x}_n$; then to advance a step twice as large is attempted, and two iterations performed. Then the difference between $(\partial\bar{u}/\partial\bar{x})^{n,m}$ and ${}^{(2)}(\partial\bar{u}/\partial\bar{x})^{n+1,m}$ is computed for all m; the $\Delta_{\bar{x}}$ is considered satisfactory if this difference, which is a measure of $(\partial^2\bar{u}/\partial\bar{x}^2)$, is such that the third term in the Taylor series expansion of $\bar{u}(\bar{x}, \bar{r})$ is 10 per cent or less of the second term. If that $\Delta_{\bar{x}}$ is found unsatisfactory according to that criterion, the $\Delta_{\bar{x}}$ is halved, and the computation repeated until a satisfactory $\Delta_{\bar{x}}$ is found. With $\Delta_{\bar{x}}$ determined the iterations proceed until two successive sets of $V^{n,m}$ values agreed with 0·1 per cent.

3. RESULTS AND DISCUSSION

We have defined variables in such a way that when molecular weights and transport properties are given, two nondimensional dynamical parameters remain in the problems, the initial Reynolds number R and the nondimensional wall injection velocity $V_w = (\bar{\rho}\bar{v})_w$. It is easy to see from the describing equations that R can be absorbed as a scale factor in $\bar{x}$ (viz., $\tilde{x} \equiv \bar{x}/R$), in such a way that only one parameter RV_w remains in the problem after molecular weights and transport parameters have been specified. To achieve the greatest generality in presenting results, we shall therefore usually employ the modified axial coordinate $\bar{x}/R$, and we shall specify RV_w instead of V_w. To check our calculation against previously reported results, computations were performed for constant-property systems $\kappa_c = 0$ for $RV_w = -5$, a case studied by Hornbeck *et al.* [2]. The present results agreed with those of Hornbeck *et al.* within the accuracy to which the curves published in [2] can be read.

Computations were also performed with $RV_w = -67{\cdot}5$ corresponding to $R = 582$, $V_w = -0{\cdot}116$, in order to compare with experimental hot-wire results for velocities obtained by Aihara† for the air-to-air case. The comparison between theory and experiment, shown in Fig. 2 is seen to be good. As may be inferred from the linearity of the computed curves for $\tilde{x} \gtrsim 0{\cdot}02$ it is seen that most of the experimental points are in the downstream asymptotic region, where Yuan's [4] similarity theory is applicable and where the velocity profile obeys a cosine-squared law.

The remaining results to be considered in this paper are for injection of nitrogen into helium (case A) and for injection of helium into nitrogen (case B), in isothermal systems at 25°C. Air differs negligibly from nitrogen for these calculations, and therefore the results also apply to helium–air systems. The differences we have observed between injection of a light gas and injection of a heavy gas can be understood in

† These experiments were performed at UCSD with with a porous tube, 30 in. long and 3 in. dia., as part of the present investigation. The authors are indebted to Dr. Aihara for making his results available to them.

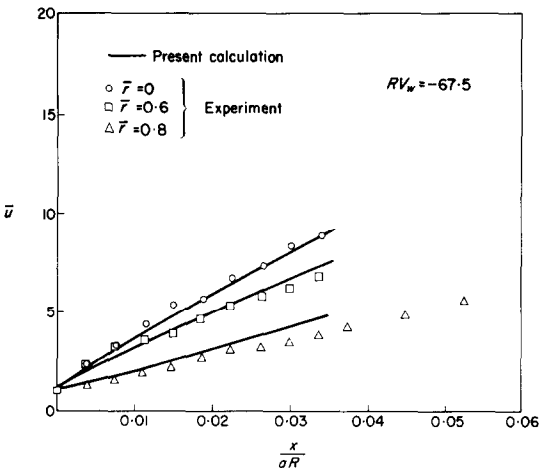

FIG. 2. The comparison of the development of velocity with experiment for homogeneous injection.

terms of the concentration profiles shown in Fig. 3. Comparison of the concentration profiles for case A (with $RV_w = -1$) with the corresponding profiles for case B clearly shows that when a light gas is injected, the concentration is considerably more uniform (at a given mass rate of injection) than when a heavy gas is injected. A light injected gas apparently can diffuse into the main stream appreciably more rapidly (in comparison with its rate of injection) than a heavy injected gas. In the case $RV_w = -1$, when the light gas is injected it diffuses sufficiently rapidly to the centerline for the centerline concentration of injectant to reach 1 per cent at $\bar{x}/R \approx 4 \times 10^{-2}$, but when the heavy gas is injected the centerline concentration of injectant does not reach 1 per cent $\bar{x}/R \approx 1{\cdot}5 \times 10^{-1}$.

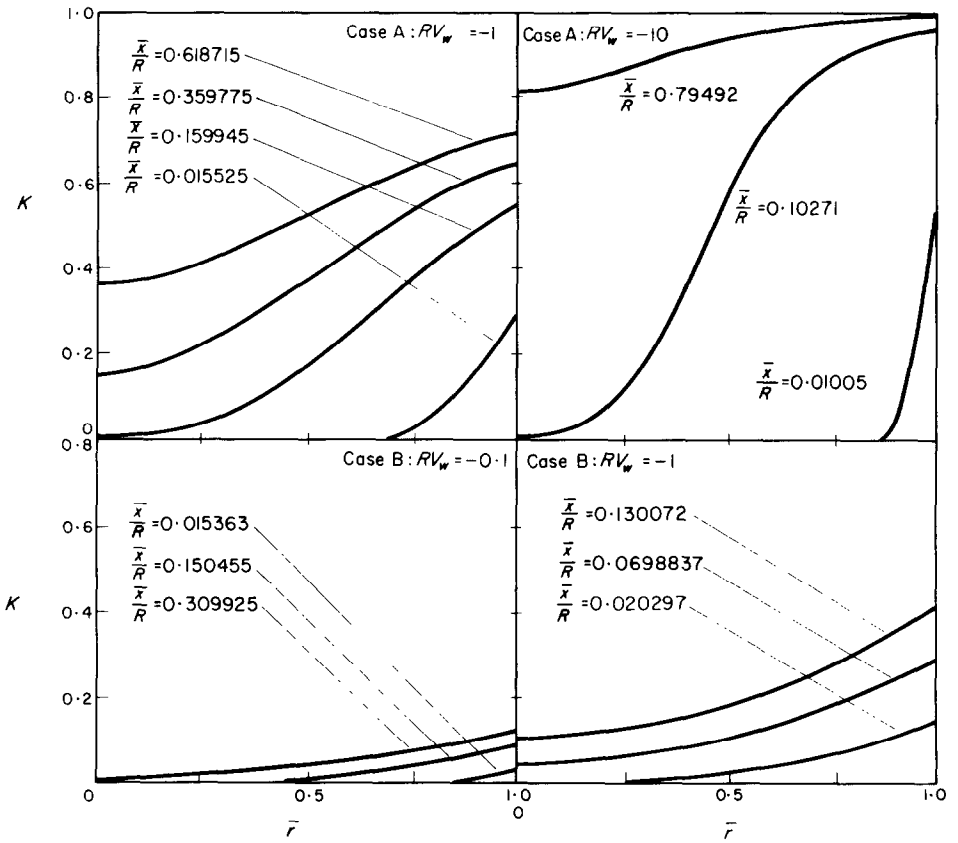

FIG. 3. The development of the concentration profile for heterogeneous injection.

An inflection point appears much sooner in the concentration profile when a heavy gas is injected (inflection appears at $\bar{x}/R \approx 10^{-1}$ for injection of heavy gas and at $\bar{x}/R \approx 3 \times 10^{-1}$ for injection of light gas in the case considered). The tendency to a greater degree of stratification with a heavier injectant will be seen later to possess a number of implications concerning velocity and pressure profiles.

The curves shown in Fig. 3 for case A with three different values of RV_w, clearly show that as the injection rate increases, concentration nonuniformities increase. The effect is quite pronounced: For $RV_w = -10^{-1}$ the composition is seen to be practically uniform across the entire cross section of the tube, at all values of $\bar{x}/R$ except the smallest (very near the entrance of the duct, a pocket of injectant with very small but measurable concentration exists next to the wall while the injectant concentration in the centre of the duct is still negligibly small). On the other hand, for $RV_w = -10$, the flow remains highly stratified for an appreciable distance from the entrance to the duct; at $\bar{x}/R = 10^{-2}$, the injectant has not yet penetrated to any significant extent to $\bar{r} = 0{\cdot}85$ and the wall concentration of injectant is approximately 0·6, and at $\bar{x}/R = 10^{-1}$ the wall concentration of injectant is nearly unity while the centerline concentration is still practically

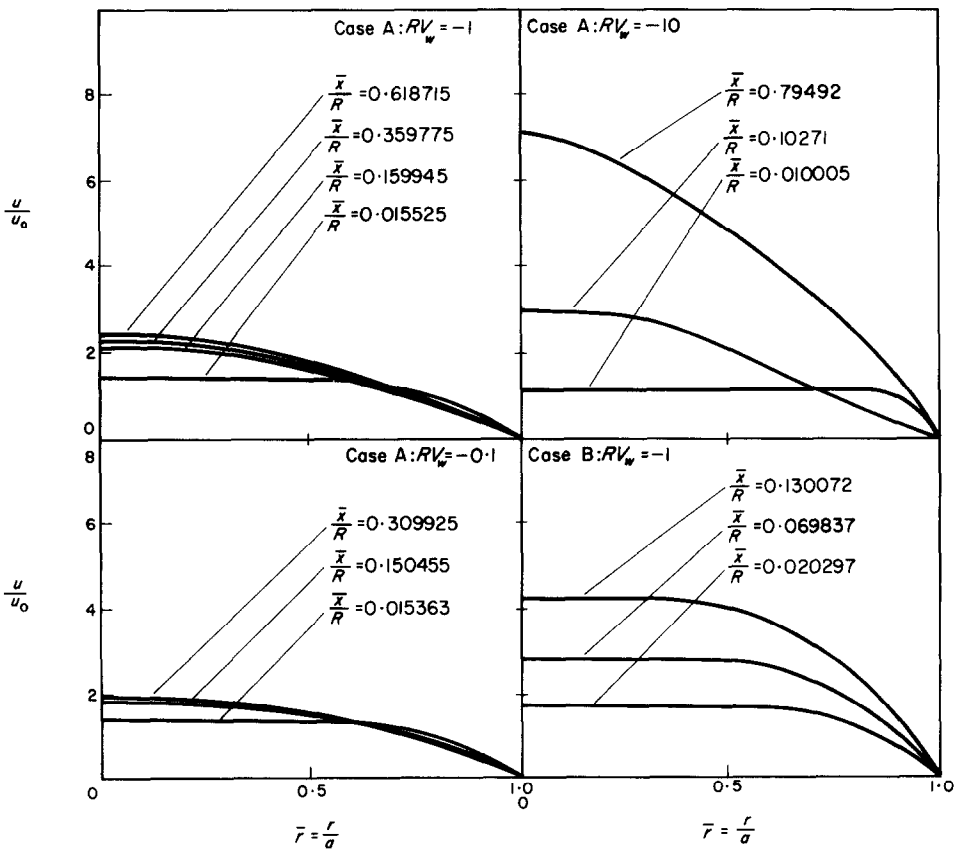

FIG. 4. The development of the velocity profiles for heterogeneous injection.

with increasing injection rate is qualitatively as might be expected on physical grounds; at higher injection rates there is less time available for diffusion to smooth out the concentration field, and this causes an increase in the ratio of radial convective mass flux of injectant to diffusive mass flux of injectant.

Velocity profiles are shown in Fig. 4 for the same four cases that were shown in Fig. 2. The velocity profiles for case A with $RV_w = -10^{-1}$ differ very little from constant-property velocity profiles at the same value of RV_w. At these small injection rates, the injectant diffuses across the duct sufficiently rapidly for composition to remain practically uniform, and the only important effect of the molecular weight of the injectant is a gradual increase (or decrease in the case of light gas injection) in the mean density of the fluid; the development length is not modified appreciably, although after fluid dynamic development is completed, the average density continues to increase gradually until it asymptotically approaches the density of the injectant, with a distance $\bar{x} = -50/V_w$ being required for the change in density to reach 99 per cent completion.

Comparison of the velocity profiles for case A with different values of RV_w shows that as the injection rate increases, the peak velocity at a given value of $\bar{x}$ increases, a result which is expected from mass conservation. However, the velocity profiles vary appreciably as RV_w changes. Moreover, the velocity profiles for case A with $RV_w = -1$ differ appreciably from those for case B with $RV_w = -1$. These differences become much less pronounced if $(\bar{\rho}\bar{u})$ profiles are plotted instead of $\bar{u}$ profiles. Thus, the peak velocity at a given value of $\bar{x}$ is larger in case B with $RV_w = -1$ than in case A with $RV_w = -1$, but the centerline density is lower in case B, so that the peak values of $(\bar{\rho}\bar{u})$ differ little. Further, the $\bar{u}$ profiles are broader in case B than in case A, but $\partial\bar{\rho}/\partial\bar{r}$ is positive in case A and negative in case B, so that the breadths of the $\bar{\rho}\bar{u}$ profiles differ little. One interesting aspect in the $\bar{\rho}\bar{u}$ profile is the existence of a maximum and an inflection point in the central part of the tube but removed from the axis (see Fig. 5). This

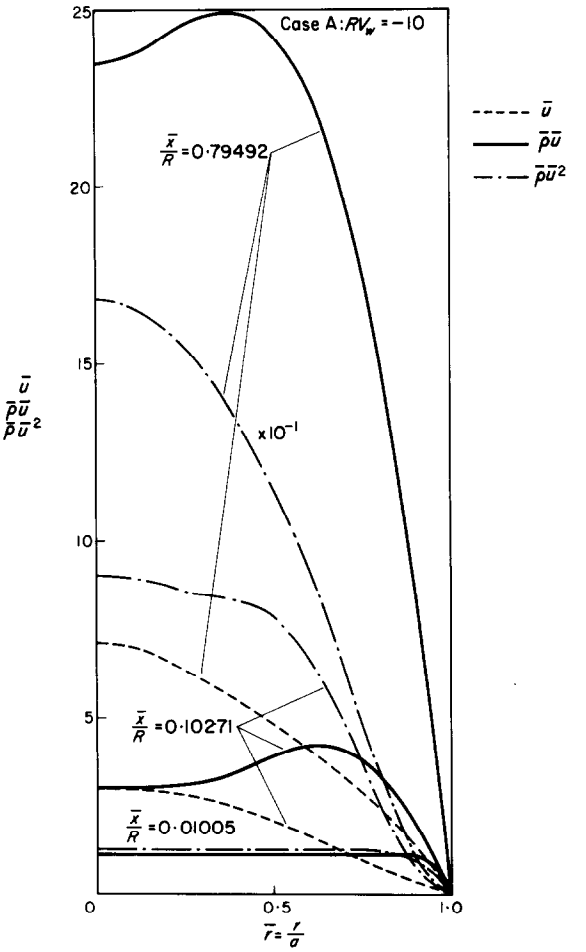

FIG. 5. The profiles of velocity, momentum and energy at various stations for case A, $RV_w = -10$.

behaviour is again traceable to the effect of density variations. The profile which differs perhaps the least from the corresponding constant-property profile is that for momentum flux $(\bar{\rho}\bar{u}^2)$.

The pressure gradients for the various cases considered are shown in Fig. 6. The qualitative shapes of the curves in Fig. 6 are consistent with previous studies; dp/dx is always negative, it is

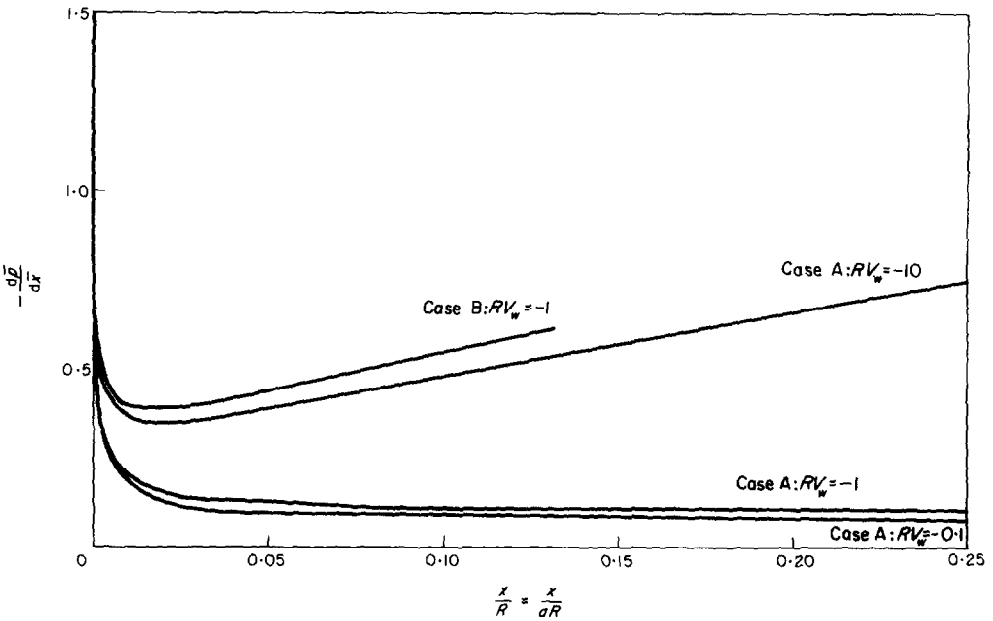

FIG. 6. The development of the pressure gradient.

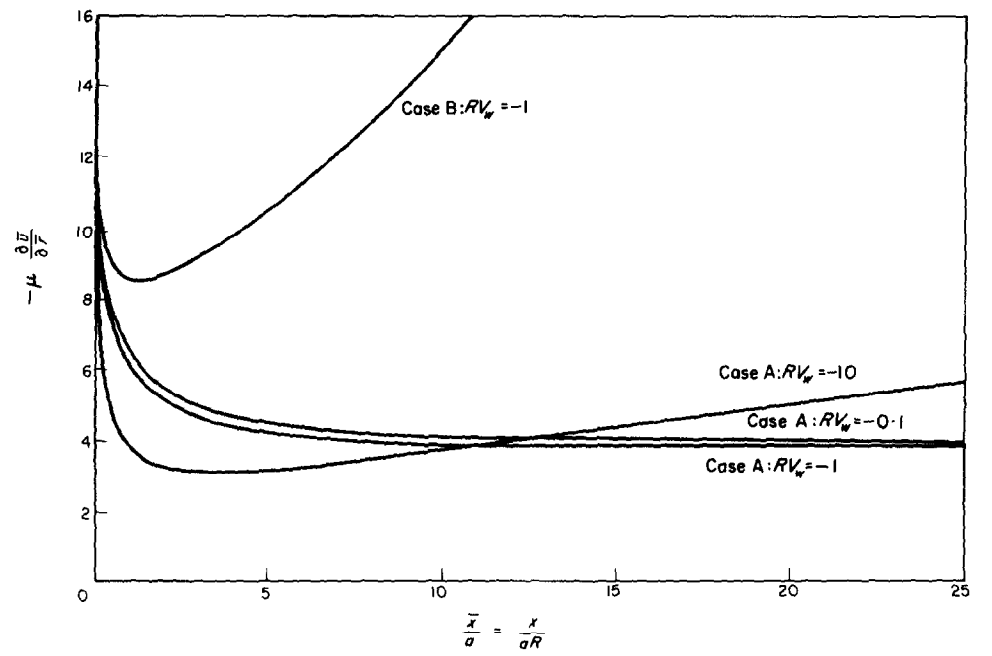

FIG. 7. The development of the shear stress.

large in magnitude near the entrance (approaching infinity as $\bar{x} \to 0$), its magnitude decreases reaching a minimum at some value of $\bar{x}$, and then its magnitude increases eventually approaching a straight line the slope of which increases with increased values of $-RV_w$ and is given by the asymptotic similarity solution of Yuan [4]. The curves in Fig. 6 show an appreciable variation from one set of conditions to another. The variation with RV_w is similar to that found earlier [2] for constant-property systems. However, the large differences between the curves for light and heavy gas injection cannot be inferred from constant-property results. Pressure gradients are appreciably larger for light gas injection than for heavy gas injection at the same rate (mass/s). This result is consistent with our observation that the $\bar{\rho}\bar{u}^2$ profiles are not affected greatly by the molecular weight of the injectant. The viscosity and velocity gradient at the wall are both influenced appreciably by the molecular weight of the injectant. Hence, the wall shear depends on the molecular weight of the injectant. Since the momentum flux profiles ($\bar{\rho}\bar{u}^2$) do not change greatly, the change in wall shear must make itself felt through the axial pressure gradient in order to conserve momentum. In Fig. 7 we show the distribution of a parameter, $\bar{\mu}(\partial\bar{u}/\partial\bar{r})$ at $\bar{r} = 1$, which provides a measure of the wall shear. We note that the comparison of Figs. 6 and 7 supports this interpretation; injection of a light gas increases the magnitude of the axial pressure gradient and increases the magnitude of the wall shear in a developing flow. The opposite effect is produced by the same mass rate of injection of a heavy gas. It is interesting to note that these effects are precisely the opposite of what is found to occur for injection into a flat-plate boundary layer.

REFERENCES

1. R. W. Hornbeck, *Appl. Sci. Res.* **13A**, 224 (1963).
2. R. W. Hornbeck, W. T. Rouleau and F. Osterle, Laminar entry problems in porous tubes, *Phys. Fluids* **6**, 1694 (1963).
3. J. O. Hirschfelder, C. F. Curtiss and R. B. Bird, *Molecular Theory of Gases and Liquids*. John Wiley, New York (1954).
4. S. W. Yuan and A. B. Finkelstein, Laminar pipe flow with injection and suction through a porous wall, *Trans. Am. Soc. Mech. Engrs* 719 (1956).
5. S. Goldstein, *Modern Developments in Fluid Dynamics*, Vol. 1, p. 305. Clarendon Press, Oxford (1938).

APPENDIX

For the initial data of interest in the present problem, corresponding as it does to the flow through a porous disc closing the tube, we effectively have a boundary layer developing on the wall of the tube with an origin at $\bar{x} = 0$, $\bar{r} = 1$. To provide initial data appropriate for our downstream marching technique we extend the Atkinson–Goldstein [5] analysis for the inlet flow to a tube to the case of mass transfer, both homogeneous and heterogeneous.

The solution near the tube entry is obtained by starting from the equation of motion [equation (1)]

$$\bar{\rho}\bar{u}\frac{\partial\bar{u}}{\partial\tilde{x}} + \bar{\rho}\tilde{v}\frac{\partial\bar{u}}{\partial y} = -\frac{\partial\bar{p}}{\partial\tilde{x}} + \frac{\partial}{\partial y}\left(\bar{u}\frac{\partial\bar{u}}{\partial y}\right) - 2\frac{\partial}{\partial y}\left(\bar{u}y\frac{\partial\bar{u}}{\partial y}\right),$$

from the equation of continuity [equation (3)]

$$(\partial/\partial\tilde{x})(\bar{\rho}\bar{u}) + (\partial/\partial y)(\bar{\rho}\tilde{v}) = 0$$

and from the equation of species conservation [equation (4)]

$$\bar{\rho}\bar{u}(\partial\kappa/\partial\tilde{x}) + \bar{\rho}\tilde{v}(\partial\kappa/\partial y) = \partial/\partial y[\mathscr{M}(\partial\kappa/\partial y)] - 2\partial/\partial y[\mathscr{M}y(\partial\kappa/\partial y)],$$

where

$$y = 1/2(1 - \bar{r}^2)$$

$$\tilde{x} = \bar{x}/R$$

$$\tilde{v} = -R\bar{v}\bar{r}.$$

Using the transformations

$$s = \int_0^{\tilde{x}} u_e \, dx,$$

$$\eta = u_e(2s)^{-1/2}\int_0^y \bar{\rho}\, dy',$$

we find

$$\frac{\partial}{\partial\eta}\left[c\frac{\partial^2 f}{\partial\eta^2}\right] + f\frac{\partial^2 f}{\partial\eta^2} + \beta(s)\left[\frac{1}{\bar\rho} - \left(\frac{\partial f}{\partial\eta}\right)^2\right] = 2s\left[\frac{\partial f}{\partial\eta}\frac{\partial^2 f}{\partial s\partial\eta} - \frac{\partial f}{\partial s}\frac{\partial^2 f}{\partial\eta^2}\right] + 2y\frac{\partial}{\partial\eta}\left[c\frac{\partial^2 f}{\partial\eta^2}\right] + 2\bar\mu\sqrt{(2s)}\frac{1}{u_e}\frac{\partial^2 f}{\partial\eta^2}$$

and

$$\frac{\partial}{\partial\eta}\left[\bar\rho\mathscr{M}\frac{\partial\kappa}{\partial\eta}\right] + f\frac{\partial\kappa}{\partial\eta} = 2s\left[\frac{\partial f}{\partial\eta}\frac{\partial\kappa}{\partial s} - \frac{\partial f}{\partial s}\frac{\partial\kappa}{\partial\eta}\right] + 2y\frac{\partial}{\partial\eta}\left[\bar\rho\mathscr{M}\frac{\partial\kappa}{\partial\eta}\right] + 2\mathscr{M}\frac{\sqrt{(2s)}}{u_e}\frac{\partial\kappa}{\partial\eta},$$

where

$$\bar\rho\bar u = \partial/\partial y[\sqrt{(2s)}f]$$
$$\bar\rho\bar v = -\partial/\partial\bar x[\sqrt{(2s)}f]$$
$$c = \bar\rho\bar\mu$$
$$\beta(s) = (2s/u_e)\,\mathrm{d}u_e/\mathrm{d}s).$$

The boundary conditions become

$$f(s,0) = -1/\sqrt{(2s)}\int_0^s \frac{(\rho\bar v)_w}{u_e}\,\mathrm{d}s,$$

$$\partial f/\partial\eta(s,0) = 0,$$

$$\partial f/\partial\eta(s,\infty) = 1,$$

$$\bar\rho u_e(\partial\kappa/\partial\eta)(s,0) = -\sqrt{(2s)}\,Sc(\bar\rho\bar v)_w(\kappa_c - \kappa_w)$$

$$\kappa(s,\infty) = 0$$

Generalizing the method of Atkinson and Goldstein [5] to flows of binary gas mixtures with wall injection we consider a series expansion

$$f(s,\eta) = f_0(\eta) + \sqrt{(2s)}f_1(\eta) + \ldots$$
$$\kappa(s,\eta) = \sqrt{(2s)}\kappa_1(\eta) + \ldots$$
$$\bar\rho^{-1}(s,\eta) = 1 + \sqrt{(2s)}w_1\kappa_1(\eta) + \ldots$$
$$c(s,\eta) = 1 + (\partial c/\partial\kappa)_{\kappa=0}\sqrt{(2s)}\kappa_1(\eta) + \ldots,$$
$$\bar\rho\mathscr{M} = \mathscr{M}_0 + (\partial\bar\rho\mathscr{M}/\partial\kappa)_{\kappa=0}\sqrt{(2s)}\kappa_1(\eta) + \ldots,$$

and couple the external flow to the boundary layer by applying conservation of mass at each station $\bar x$; thus we have

$$u_e = 1 + 2\sqrt{(2s)}\int_0^\infty (1 - f_0')\,\mathrm{d}\eta + 2s\left[(\rho\bar v)_w + 2\int_0^\infty (w_1\kappa_1 - f_1')\,\mathrm{d}\eta\right] + \ldots$$

$$\beta(s) = 2\sqrt{(2s)}\int_0^\infty (1 - f_0')\,\mathrm{d}\eta + 4s\left\{(\rho\bar v)_w + 2\int_0^\infty (w_1\kappa_1 - f_1')\,\mathrm{d}\eta - \left[\int_0^\infty (1 - f_0')\,\mathrm{d}\eta\right]^2\right\}.$$

Substituting into the full equations and equating coefficients of powers of $\sqrt{(2s)}$ yields the following equations for the f's and κ_1:

$$f_0''' + f_0 f_0'' = 0,$$
$$f_0(0) = f_0'(0) = 0, \qquad f_0'(\infty) = 1$$
$$\mathscr{M}_0\kappa_1'' + f_0\kappa_1' - f_0'\kappa_1 = 0$$
$$\kappa_1'(0) = -S_{c,w}(\bar\rho\bar v)_w\kappa_c$$
$$\kappa_1(\infty) = 0$$
$$f_1''' + f_0 f_1'' - f_0' f_1' + 2f_0'' f_1 = -2\left[\int_0^\infty (1 - f_0')\,\mathrm{d}\eta\right][1 - f_0'^2] - (\partial c/\partial\kappa)_{\kappa=0}f_0''(\kappa_1' - f_0\kappa_1) + 2\eta f_0''' + 2f_0''$$
$$f_1(0) = -(\bar\rho\bar v)_w/2 \quad f_1'(0) = 0 \quad f_1'(\infty) = 0.$$

It is seen that f_0 is the well-known Blasius function and that succeeding equations are linear. The two-point boundary-value problems for κ_1 and f_1 can therefore be reduced to one-point boundary-value problems. The ordinary differential equations so reduced were solved numerically by a forward integration routine. The solutions for f_1 and κ_1 depend on the flow parameters $(\bar\rho\bar v)_w$ and κ_c and on the gas properties in $\mathscr{M}_0$, $S_{c,w}$, and $(\partial c/\partial\kappa)_{\kappa=0}$ and they provide velocity and concentration profiles in the boundary layer that develop on the wall near the entrance of the duct.

We are interested not only in the profiles which provide the initial data for the numerical solution but in the velocity in the core, u_e; this can be expanded as

$$u_e = 1 + c_1(\tilde{x})^{1/2} + c_2\tilde{x} + \ldots$$

where

$$c_1 = 2\sqrt{2}\int_0^\infty (1 - f'_0)\,d\eta = 3{\cdot}441576$$

$$c_2 = 4\{w_1\int_0^\infty \kappa_1\,d\eta - f_1(\infty) + 2/3\,[\int_0^\infty (1 - f'_0)\,d\eta]^2\}.$$

The coefficients c_1 and c_2 correspond to the constants κ_1 and κ_2 of [5]. The value of c_1 is of course numerically equal to κ_1, but the values of c_2 differ from $\kappa_2 = -9{\cdot}0938$ because of injection. Values of c_2 for various cases are given in Table A.1. We remark that numbers shown for light gas injection with $(\bar{\rho}\bar{v})_w = -0{\cdot}1$ may not be physically meaningful because the boundary-layer approximation may break down.

Now the value of $\tilde{x}$ at which the numerical solution is started must be determined by the requirement that $|c_2(\tilde{x}_i)^{1/2}| \ll |c_1|$. Typically $\tilde{x}_i = 0(10^{-5})$ and a fine radial mesh corresponding to $\delta_r = 1/200$ had to be used in order to obtain adequate resolution of the initial data. As the numerical solution proceeded downstream grid points were dropped until the standard mesh of $\delta_r = 1/40$ quoted above could be employed.

Table A.1

W_1	W_2	RV_w	$(\bar{\rho}\bar{v})_w$ for $R = 100$	c_2
28	4	−10	−0·1	−49·22
28	4	−1	−0·01	−12·54
28	4	−0·1	−0·001	−6·357
28	28	−5	−0·05	17·04
4	28	−10	−0·1	1899
4	28	−1	−0·01	9·102
4	28	−0·1	−0·001	−9·003

Résumé—Les écoulements laminaires isothermes à l'entrée de tuyaux de section droite circulaire avec une vitesse uniforme d'injection massique à la paroi sont calculés à partir des équations de la couche limite par une technique de différences finies implicites.

On décrit les résultats pour des systèmes avec un poids moléculaire constant, pour l'injection d'un gaz léger dans un gaz lourd, et pour l'injection d'un gaz lourd dans un gas léger, en insistant spécialement sur les mélanges hélium–azote. On tient compte convenablement de la dépendance de la masse volumique et de la viscosité enfonction de la composition. L'effet du poids moléculaire sur l'établissement de l'écoulement et sur le mélange est discuté.

Zusammenfassung—Laminare, isotherme Einlaufströmungen in Kanälen von kreisförmigen Querschnitt mit gleichförmiger Stoffzugabe an der Wand werden mit Grenzschichtgleichungen nach einem impliziten endlichen Differenzenverfahren berechnet. Ergebnisse werden angegeben für Systeme mit konstantem Molekulargewicht, für die Zugabe eines leichten Gases in ein schweres und für die Zugabe eines schweren in ein leichtes Gas mit einem Schwerpunkt auf Helium–Stickstoffgemischen.

Die Abhängigkeit der Dichte und Zähigkeit von der Zusammensetzung wird genau berücksichtigt. Der Einfluss des Molekulargewichts auf die Strömung und Vermischung wird diskutiert.

Аннотация—Рассчитывается ламинарное изотермическое течение во входном участке каналов круглого поперечного сечения при равномерном вдуве на стенке. Уравнения пограничного слоя решались при помощи неявной конечно-разностной схемы. Представлены результаты для систем с постоянным молекулярным весом, при вдуве легкого газа в тяжелый газ и тяжелого газа в легкий. Особое внимание уделяется смесям гелий-азот. Учитывается зависимость плотности и вязкости от состава газа. Рассматривается влияние молекулярного веса на развитие потока и смешивание.